UDC 534.4
MSC 74B10
Вестник СПбГУ. Прикладная математика. Информатика... 2023. Т. 19. Вып. 1

# Sound synthesis approach based on the elastic stress analysis of a wrinkled thin film coating*

*S. A. Kostyrko, B. S. Shershenkov*

ITMO University, 49, Kronverksky pr., St. Petersburg, 197101, Russian Federation

**For citation:** Kostyrko S. A., Shershenkov B. S. Sound synthesis approach based on the elastic stress analysis of a wrinkled thin film coating. *Vestnik of Saint Petersburg University. Applied Mathematics. Computer Science. Control Processes*, 2023, vol. 19, iss. 1, pp. 72–89.
https://doi.org/10.21638/11701/spbu10.2023.107

This paper examines the ability to employ the model of a wrinkled thin film coating under plane strain conditions for the generation and manipulation of sounds. It is assumed that the film-on-substrate structure represents a multilevel system consisting of four phases with different elastic properties such as surface layer, film material, interphase and substrate material. The undulation of surface and interface geometry leads to the complex stress state of the film coating resulting from the superposition of two perturbed stress fields evolved near the curved surface and interface. The analysis of the stress state reveals the periodic distribution of the longitudinal stresses smoothly changing from surface to interface. This facilitates the creation of a sound synthesis technique similar to the timbre morphing method which provides the transition between two waveforms while creating new intermediate waveform during this process. The perspective of using the wrinkled thin film model for sound generation is gained by its complex behavior, where the influence of one parameter on the stress distribution is affected by other parameters, which in turn reflects in the rich sound morphologies during the mapping of the stress oscillations onto sound.

*Keywords*: sound synthesis, physical modeling approach, wrinkled thin film, stress field perturbation.

**1. Introduction.** In the last decades, many studies have been conducted developing the physical modelling approaches in the context of sound design and computer music applications [1–4]. The main efforts have been focused on the simulation of electronic circuits [5, 6], vibrating objects [7, 8], and acoustic environments [9, 10]. As it was demonstrated in [11–14], the physical models also can be used for compositional purposes extending the algorithmic music practices and bringing some benefits to interactive composing tasks such as generation and control of sound patterns and structures in real-time [15, 16]. In general, the models of sound generation and transformation based on physical principles offer new methods for performance and composition process with intuitive parametric control over a complex timbral behaviour, which explains their popularity.

Motivated by this idea, we decided to incorporate the latter research on the mechanical behaviour of ultra-thin films with a thickness in the range of 1–100 nm into the framework of sound synthesis algorithms. In recent years, the development of low-defect nanocomposites became one of the priority areas of modern micro- and optoelectronics. By combining materials and structural elements at the nanoscale, it is possible to create devices with unique optical, electrical and magnetic properties [17, 18]. It is well known that the mechanical properties of materials at the nanoscale highly depend on the size of

* This work was supported within ITMO Fellowship Program.

the structural elements [19]. The increased ratio of surface area to volume increases the role of surface and interface layers in the mechanical performance of such materials [20]. It is generally believed that the elastic properties of the surface and interphase layers differ substantially from similar properties of the bulk phases [21, 22]. At the macrolevel, this difference practically does not affect the properties and behaviour of the solids. However, in the case of nanostructures, this difference is manifested, in particular, in the noticeable influence of surface and interface stresses on the physical properties of the material [23, 24]. The calculations carried out using the molecular dynamics simulations confirmed this hypothesis and allowed the developing an approach describing a deformable solid as a multilevel system where the surface and interphase layers are considered as the separate subsystems that have physical and mechanical properties different from the bulk material [25, 26].

Thus, one of the most important directions for research in the field of thin-film mechanics is connected with the development of theoretical models for accurate measuring and analysis of the stress state in ultra-thin film materials that take into account the effect of surface and interface stresses. In view of this problem, we have been working on the continuum models capable to predict the distribution of stresses in ultra-thin film coatings with periodically perturbated surface and interface profiles [27–33]. It should be noted that the experimental studies and numerical simulations revealed a large number of possible roughening scenarios during deposition and consequent annealing process of the thin film materials [32, 33]. One of the mechanisms resulting in perturbation of thin film geometry is buckling driven by mechanical instability which is commonly observed in thin-film structures with compliant substrates under compressive loading [34, 35]. Another one is related to the morphological changes at the atomic level as a consequence of stress field relaxation [36–38]. The dominant driving force of such transformations is a change in the chemical potential, which, due to the reduced stability of the surface atomic layers, leads to the diffusion of atoms along the surface with a high value of the chemical potential to the regions with a low value [39]. This process leads to the formation of a nano- and microrelief which dramatically alter the further performance of micro- and optoelectronic devices affecting their mechanical, electrical and optical properties [17]. Therefore, it is important from both the fundamental and technological point of view to understand how the topological and elastic properties of the surface and interface influence on the stress distribution in ultra-thin film materials.

For this purpose, the theoretical framework was developed based on surface/interface elasticity model proposed by Gurtin and Murdoch [40, 41]. They offered to consider the surface and interphase domains of heterogeneous solids as negligibly thin layers ideally adhering to the bulk materials and differing from them by the elastic moduli. The stress resultants acting in such surface/interface layers were considered as surface/interface stresses. This allowed deriving the constitutive equations linked the surface/interface stress and strain tensors. The conditions of mechanical equilibrium on the surface and interface were given in the terms of generalized Young — Laplace equations [42]. The additional boundary equations were introduced from the inseparability conditions of bulk and surface/interface domains. To solve these equations jointly with the constitutive equations of Hooke law describing the elastic behaviour of film and substrate bulk materials, we employ the complex variable method [43–45] and boundary perturbation technique [46] whereby the unknown functions are sought in the form of a power series in the small parameter represented by an amplitude-to-wavelength ratio of surface/interface relief. This led to semi-analytical expressions for the components of the stress and strain tensors derived in the form of Fourier

series. The subsequent numerical analysis provides an opportunity to investigate the effect of geometrical and physical parameters on stress distribution in ultra-thin film coating. The most interesting results were obtained in the case when both free surface and interface were undulated [30]. Such configuration leads to the superposition of two perturbed stress fields raised as a result of surface and interface perturbation. Consequently, the interference patterns occur in the stress field within the bulk phase of the film coating. This means that calculating the stress distribution along the lines parallel to the unperturbed surface/interface boundaries we get different waveforms smoothly changing from surface to interface. In terms of sound synthesis techniques, this reminds the timbre morphing method which provides transition between two sounds while creating new intermediate sounds during this process [47, 48]. In fact, that comparison led us to the idea to apply the model of ultra-thin film coating with perturbed surface and interface for sound synthesis perspectives. However, it should be noted that it has some other features related to the complex behaviour of multilevel systems where the influence of one parameter on stress distribution is affected by other parameters. All these aspects are emphasized in this paper considering the stress distribution in terms of sound representation.

**2. Elasticity problem.** Consider an ultra-thin film coating with undulated geometry bonded to a substrate under plane strain conditions which means that there is zero strain in the direction normal to the axis of applied stress (Figure 1). This allows us to formulate a two-dimensional boundary value problem for a curvilinear strip $\Omega_1$ of an arbitrary thickness $h_f$ bonded to a half-plane $\Omega_2$. Introducing a complex variable $z = x_1 + \mathrm{i}x_2$, where $\mathrm{i}^2 = -1$ and $(x_1, x_2)$ are the global Cartesian coordinates, the undulated geometry of the film is described by the continuous function $f$ as it follows:

$$\begin{gathered}\Gamma_1 = \{z : z \equiv z_1 = x_1 + \mathrm{i}[h_f + \varepsilon f(x_1)]\}, \\ \Gamma_2 = \{z : z \equiv z_2 = x_1 + \mathrm{i}\varepsilon f(x_1)\}, \\ \Omega_1 = \{z : \varepsilon f(x_1) < x_2 < h_f + \varepsilon f(x_1)\}, \\ \Omega_2 = \{z : x_2 < \varepsilon f(x_1)\},\end{gathered} \tag{1}$$

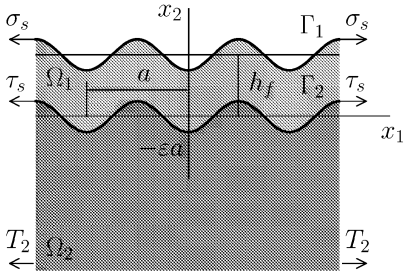


*Figure 1.* Schematic of the wrinkled film coating

where $f(x_1 + a) = f(x_1)$, i. e. $a$ is the wavelength of undulation, the maximum deviation of the film from a flat configuration is $A = \varepsilon a$, i. e. $\max|f(x_1)| = A$, and $\varepsilon$ is a perturbation parameter.

Under the condition of infinitesimal deformation in the case of plane strain, the constitutive equations describing the stress-strain relations for surface/interphase layers and bulk phases of the elastically isotropic film-substrate system reduce to

$$\begin{gathered}\sigma^s_{tt}(z_j) = M^s_j \varepsilon^s_{tt}(z_j), \;\; \sigma^s_{33}(z_j) = \lambda^s_j \varepsilon^s_{tt}(z_j), \\ M^s_j = \lambda^s_j + 2\mu^s_j, \;\; z_j \in \Gamma_j, \;\; j = \{1, 2\},\end{gathered} \tag{2}$$

$$\begin{aligned}\sigma_{nn}(z) &= (\lambda_j + 2\mu_j)\varepsilon_{nn}(z) + \lambda_j \varepsilon_{tt}(z), \\ \sigma_{tt}(z) &= (\lambda_j + 2\mu_j)\varepsilon_{tt}(z) + \lambda_j \varepsilon_{nn}(z), \\ \sigma_{33}(z) &= \frac{\lambda_j}{2(\lambda_j + \mu_j)} \left[\sigma_{tt}(z) + \sigma_{nn}(z)\right],\end{aligned} \tag{3}$$

$$\sigma_{nt}(z) = 2\mu_j \varepsilon_{nt}(z),\ z \in \Omega_j,\ j = \{1, 2\},$$

here $\sigma^s_{tt}$ and $\varepsilon^s_{tt}$ are the surface/interface stress and strain, $\{\sigma_{nn},\ \sigma_{tt},\ \sigma_{nt}\}$ and $\{\varepsilon_{nn},\ \varepsilon_{tt},\ \varepsilon_{nt}\}$ are the components of bulk stress and strain tensors defined in the local Cartesian coordinates $(n, t)$, $\mathbf{n}$ and $\mathbf{t}$ are normal and tangential to the interface; $\{\lambda^s_j,\ \mu^s_j\}$ and $\{\lambda_j,\ \mu_j\}$ are the Lamé constants for surface/interphase layer $\Gamma_j$ and bulk phase $\Omega_j$, respectively.

It is supposed that the presence of surface $\sigma^s$ and interface $\tau^s$ stresses results in surface traction $\sigma(z_1)$ and traction jump $\Delta\sigma(z_2)$ across the interface according to the generalized Young—Laplace law:

$$\begin{aligned} \sigma(z_1) =& T^s \sigma^s(z_1), \\ \Delta\sigma(z_2) = \sigma^+(z_2) - &\sigma^-(z_2) = -T^s \tau^s(z_2), \end{aligned} \tag{4}$$

where

$$\begin{gathered} \sigma^s(z_1) \equiv \sigma^s_{tt}(z_1),\ \tau^s(x_1) \equiv \sigma^s_{tt}(z_2), \\ T^s(\cdot) = \kappa(x_1)(\cdot) - \mathrm{i}\frac{1}{h(x_1)}\frac{d(\cdot)}{dx_1}, \\ \sigma = \sigma_{nn} + \mathrm{i}\sigma_{nt},\ \sigma^{\pm}(z_2) = \lim_{z \to z_2 \pm \mathrm{i}0} \sigma(z), \end{gathered}$$

and $\kappa$ and $h$ are the local principal curvature and the metric coefficient, respectively.

For geometrically coherent surface and interface regions, the condition of continuity of the displacement field takes the subsequent form

$$\varepsilon^s_{tt}(z_1) = \varepsilon_{tt}(z_1), \quad \Delta u(z_2) = u^+(z_2) - u^-(z_2) = 0, \tag{5}$$

here $u^{\pm}(z_2) = \lim\limits_{z \to z_2 \pm \mathrm{i}0} u(z)$, $u = u_1 + \mathrm{i}u_2$, $u_1$ and $u_2$ are the displacements along the corresponding coordinate axes $x_1$ and $x_2$.

Due to mismatch between crystal lattice parameters of the film and substrate, the misfit stresses arise described as the far-field stress state:

$$\begin{aligned} \lim_{x_2 \to -\infty} (\sigma_{22} - &\mathrm{i}\sigma_{12}) = 0, \\ \lim_{x_2 \to -\infty} \sigma_{11} = T_2, &\quad \lim_{x_2 \to -\infty} \omega = 0, \end{aligned} \tag{6}$$

where $\sigma_{ij}$ $(i, j = \{1, 2\})$ are the stresses in coordinates $(x_1, x_2)$ and $\omega$ is the rotation angle.

Since it is supposed that the film and substrate materials are linearly elastic, the boundary value problem (1)–(6) can be solved on the basis of the superposition principle employing the solutions derived recently in terms of Goursat—Kolosov complex potentials [49, 50]. Following this technique, the solution for the film-substrate system is considered as a sum of the solutions of two complementary problems. In the first problem, the bulk stresses $\sigma^1$, the surface stresses $\vartheta_{\mathbf{s}}$, and displacements $u^1$ arise under the unknown self-balanced surface load $p$ applied to the curvilinear boundary of homogeneous half-plane $D^1_1 = \{z : x_2 < h_{\mathrm{f}} + \varepsilon f(x_1)\}$ with the elastic properties of the film. The second problem describes a coupled deformation of two joint half-planes $D^2_1 = \{z : x_2 > \varepsilon f(x_1)\}$ and $D^2_2 = \{z : x_2 < \varepsilon f(x_1)\}$ with the unknown jumps of stresses $\Delta\sigma^2$ and displacements $\Delta u^2$ along the curvilinear interface under the influence of interface stresses $\tau_s$ and longitudinal ones $T_j$ acting in $D^2_j$, $j = \{1, 2\}$.

Thus, the boundary value problem (1)–(6) is reduced to the system of the boundary equations for the unknown functions $p$, $\vartheta_{\mathbf{s}}$, $\sigma_s$ and $\tau_s$. Following Kolosov [44] and Muskhelishvili [45], the stress-strain state of the elastic half-plane $D_1^1$ and two-component plane $\bigcup_{j=1}^{2} D_j^2$ is described in terms of two arbitrary holomorphic functions of a complex variable $\Phi_j^k$ and $\Upsilon_j^k$ ($k,\ j=1$ and $k=2, j=\{1,2\}$, correspondingly), the Goursat — Kolosov complex potentials. After that, the derived boundary equations are expressed as the functional equations on the boundary values of complex potentials $\Phi_j^k$ and $\Upsilon_j^k$ at curved surface $\Gamma_1$ and interface $\Gamma_2$ [30]. To obtain the solution, we utilise the boundary perturbation method which reduces the boundary conditions along the curvilinear surface and interface profiles to the equivalent ones along the rectilinear boundaries, i. e. $z_1 = x_1 + \mathrm{i}h_f$ and $z_2 = x_1$, respectively [46]. According to this method, the unknown functions are sought in the form of the power series in the small parameter $\varepsilon$:

$$\begin{gathered}\Psi(z) = \sum_{m=0}^{\infty} \frac{\varepsilon^m}{m!}\Psi_{(m)}(z), \quad \Psi(z) \equiv \{\Phi_j^k(z), \Upsilon_j^k(z)\}, \\ \Pi(z_j) = \sum_{m=0}^{\infty} \frac{\varepsilon^m}{m!}\Pi_{(m)}(z_j), \quad \Pi(z_j) \equiv \{p(z_1), \vartheta_s(z_1), \sigma_s(z_1), \tau_s(z_2)\}.\end{gathered} \tag{7}$$

And their boundary values are represented in the form of the Taylor series in the vicinity of the lines $\Im z_1 = 0$ and $\Im z_2 = 0$ treating the real variable $x_1$ as a parameter:

$$\begin{gathered}\Lambda_{(m)}(z_j) = \sum_{l=0}^{\infty} \frac{[\mathrm{i}\varepsilon f(x_1)]^l}{m!}\Lambda_{(m)}^{(l)}(x_1), \\ \Lambda_{(m)}(z_j) \equiv \{\Phi_{j(m)}^k(z_j), \Upsilon_{j(m)}^k(z_j), p_{(m)}(z_1), \vartheta_{s(m)}(z_1), \sigma_{s(m)}(z_1), \tau_{s(m)}(z_2)\}.\end{gathered} \tag{8}$$

Substituting the series (7) and (8) into the boundary equations related to the conditions of the mechanical equilibrium (4) and equating the coefficients of like powers of $\varepsilon$, we come to the recurrent sequence of equations written in the form of the Riemann — Hilbert problems on the jumps of analytical functions $\Phi_{j(m)}^k$ and $\Upsilon_{j(m)}^k$ at the rectilinear boundaries. The solution of the obtained equations gives the explicit expressions for $\Phi_{j(m)}^k$ and $\Upsilon_{j(m)}^k$ written in the form of Cauchy-type integrals on the unknown functions $p_{(m)}$, $\sigma_{s(m)}$, $\vartheta_{s(m)}$ and $\tau_{s(m)}$. By applying the derived expressions and the Sokhotski — Plemelj formulas for the limiting values of the Cauchy-type integrals [43, 51] to the boundary equations associated with the kinematic conditions (5), we come to the hypersingular integral equations in the unknown functions $p_{(m)}$, $\vartheta'_{\mathbf{s}(m)}$, $\sigma'_{s(m)}$ and $\tau'_{s(m)}$. The kernels of derived integral equations are the same for each order of the approximation, and the right-hand sides are the known continuous functions. Taking into account the properties of Cauchy-type integrals, the solution is received in the form of Fourier series.

In the Section 3, several representative numerical examples are employed to demonstrate the effect of physical and geometrical parameters on longitudinal stress $\sigma_{tt}$ distribution in ultra-thin film coating with perturbed geometry. After that, the approach to sound generation based on the developed model is discussed.

**3. Sound synthesis approach.** To begin, let us consider the metal-on-metal heteroepitaxial system with equal Poisson ratios $\nu_1 = \nu_2 = 0.3$. This assumption allows to investigate the effect of the substrate on the undulation of the stress field in the wrinkled film through the only one parameter, film-to-substrate stiffness ratio $r = \mu_1/\mu_2$. For

example, the substrate is stiffer than the film when $r < 1$, and inversely when $r > 1$. In the case when $r = 1$, we get the solution for the homoepitaxial film-on-substrate system. The surface and interface effects are presented by the elastic constants $\{\lambda_1^s,\ \mu_1^s\}$ and $\{\lambda_2^s,\ \mu_2^s\}$, respectively, which are usually determined from the molecular dynamics simulations [26, 52]. For instance, the aluminium free surface is described by the parameters $\lambda^s = 6.851$ N/m and $\mu^s = -0.376$ N/m (as a consequence $M_s = 6.099$ N/m). It should be noted that surface and interface elastic properties of thin film materials are highly dependent on fabrication and post-processing techniques. So, we take into account the effect of surface and interface elasticity through variation of constants $M_1^s$ and $M_2^s$ within the specified limits. To describe the geometry of the wrinkled thin film with arbitrary wavelength $a$, amplitude $A = a\varepsilon$ and thickness $h_f$ in accordance with equation (1), we adopt the cosine function:

$$f(x_1) = -a\cos(b_1 x_1),\ \ b_k = \frac{2\pi k}{a}.$$

Here, we restrict attention to the amplitude-to-wavelength ratio range $\varepsilon \in [0, 0.1]$ and obtain the $5^{th}$-order approximation solution:

$$\sigma_{tt}(x_1, x_2) = T_1 + \sum_{k=1}^{5} \varepsilon^k \left[A_k^0 + A_k(x_2, h_f, a, \nu_1, \nu_2, r, M_1^s, M_2^s, T_1)\cos(b_k x_1)\right].$$

The analysis similar to the one conducted in [31] estimates the convergence of the derived $5^th$-order approximate solution for $\varepsilon \in [0, 0.1]$. However, it is important to note that the accuracy of the approximation scheme decreases with the increasing of the parameter $\varepsilon$ and the higher order terms within the boundary perturbation method should be considered for its extended range.

Figure 2, *I–VIII* illustrates the distribution of the normalized longitudinal stress $\sigma_{tt}/T_1$ in the film coating along the lines parallel to the unperturbed surface/interface boundaries, i. e. $x_2 = lh_f$, $l = [0, 1]$. The distribution is plotted within one period, i. e. $x_1/a \in [-0.5, 0.5]$, for film-on-substrate systems described by the following set of parameters $a = 10$ nm, $A = \{0.05a, 0.1a\}$, $h_f = \{0.1a, 0.2a\}$, $r = \{0.1, 10\}$, $M_1, M_2 = \{1, 10\}$ N/m. Here, we don't provide a detailed analysis of the influence of various parameters on the stress distribution and emphasize only the main trends which may be of interest in the framework of model-based sound generation. First of all, we should note that increasing of the amplitude of the wrinkles $A$ leads to increasing of the stress level and change of distribution waveform (in Figure 2, compare *I* with *II*, and *V* with *VI*). The change of the stiffness ratio from $r = 0.1$ to $r = 10$ corresponding to soft and stiff film, respectively, results in a significant change of the stress distribution waveform in the bottom part of the film (in Figure 2, compare in pairs *I–IV* with *V–VIII*), which also affects the stress distribution in the top part due to the superposition of two undulated stress fields caused by perturbation of interface and free surface. The similar effect on the stress distribution in sub-surface and sub-interface areas, and, as consequence, in the bulk phase of the film, have the stiffness of surface $M_1^s$ and interface $M_2^s$, respectively (in Figure 2, compare *II* with *III*, and *VI* with *VII*). However, worth noting, the effect of the interface on the stress distribution near the free surface, and vice versa, decreases with the increasing of the film thickness $h_f$ (in Figure 2, compare *III* with *IV*, and *VII* with *VIII*).

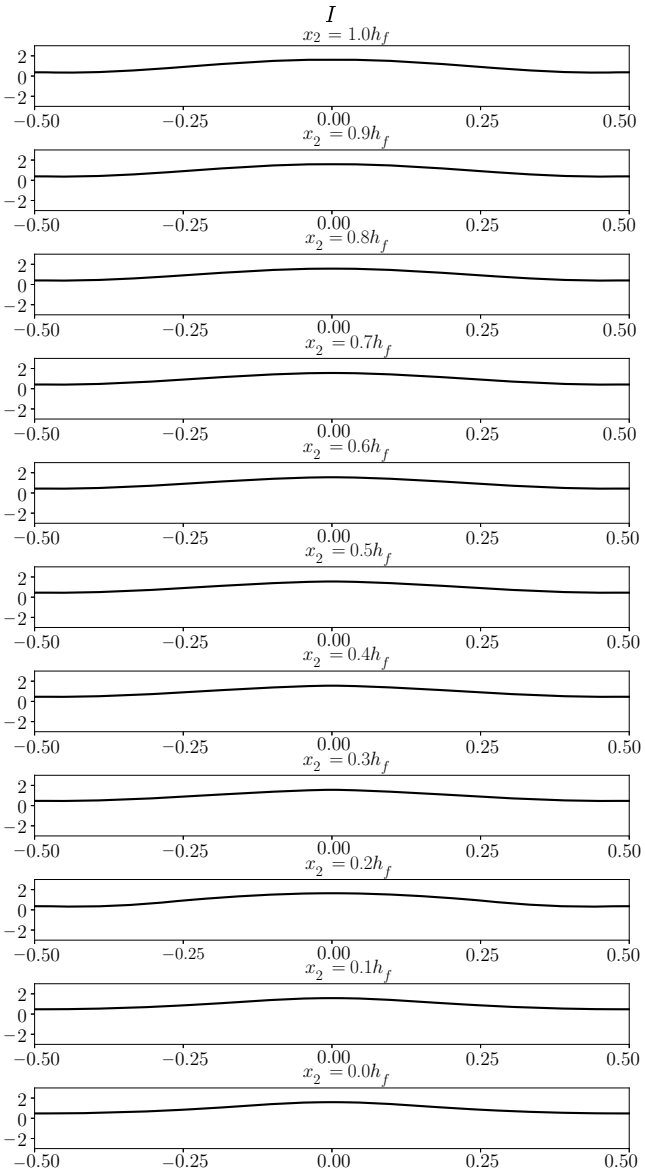


*Figure 2.* The distribution of the normalized longitudinal stress $\sigma_{tt}/T_1$ (value is plotted along the ordinate of each graph) in the film along the lines $x_2 = lh_f$, $l = [0, 1]$ (value corresponds to different graphs in a column) within one period $x_1/a = [-0.5, 0.5]$ (value is plotted along the abscissa of each graph) of a wrinkle with a wavelength $a = 10$ nm when the film-substrate system is described by the following parameters

*I*: $A = 0.05a$, $h_f = 0.1a$, $r = 0.1$, $M_1^s = 1$ N/m, $M_2^s = 1$ N/m; *II*: $A = 0.1a$, $h_f = 0.1a$, $r = 0.1$, $M_1^s = 1$ N/m, $M_2^s = 1$ N/m; *III*: $A = 0.1a$, $h_f = 0.1a$, $r = 0.1$, $M_1^s = 10$ N/m, $M_2^s = 10$ N/m; *IV*: $A = 0.1a$, $h_f = 0.2a$, $r = 0.1$, $M_1^s = 10$ N/m, $M_2^s = 10$ N/m; *V*: $A = 0.05a$, $h_f = 0.1a$, $r = 10$, $M_1^s = 1$ N/m, $M_2^s = 1$ N/m; *VI*: $A = 0.1a$, $h_f = 0.1a$, $r = 10$, $M_1^s = 1$ N/m, $M_2^s = 1$ N/m; *VII*: $A = 0.1a$, $h_f = 0.1a$, $r = 10$, $M_1^s = 10$ N/m, $M_2^s = 10$ N/m; *VIII*: $A = 0.1a$, $h_f = 0.2a$, $r = 10$, $M_1^s = 10$ N/m, $M_2^s = 10$ N/m.

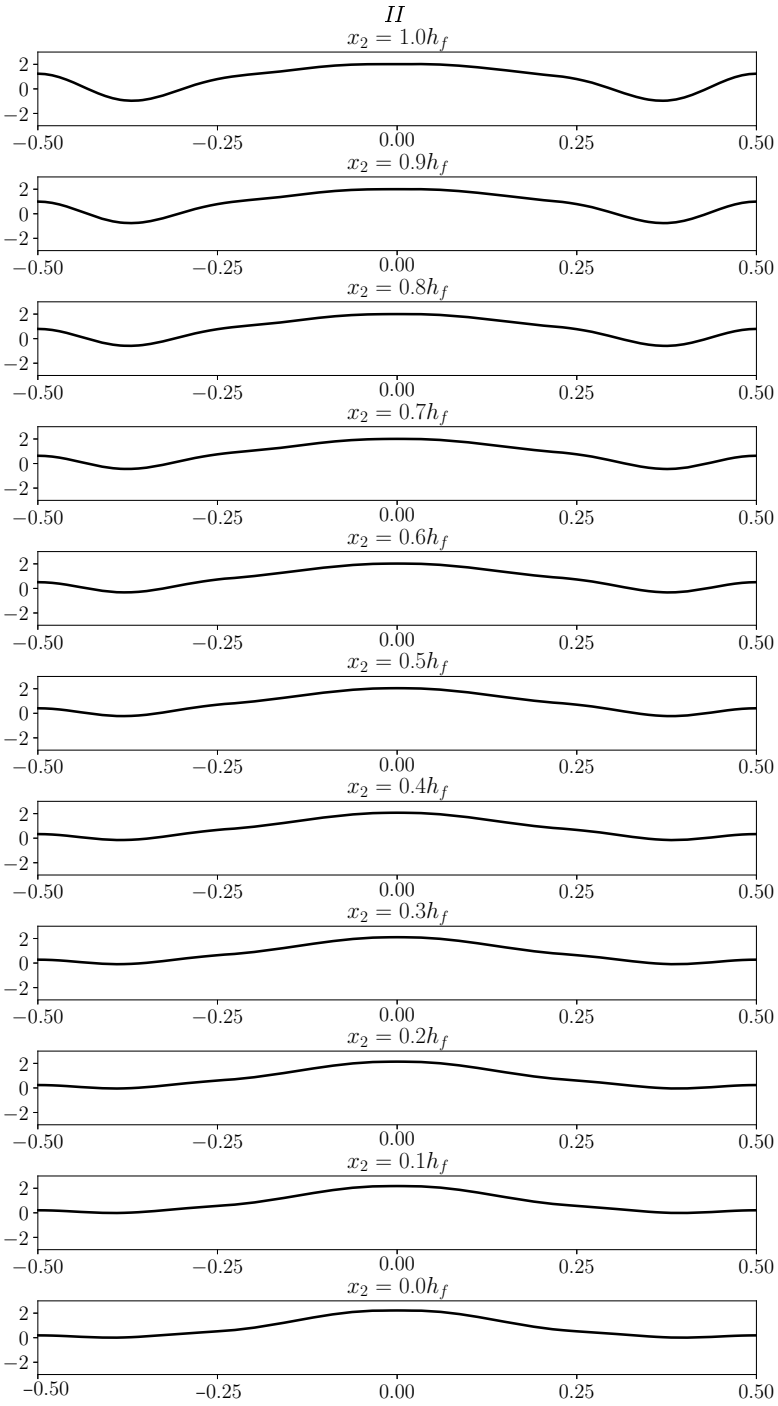


Continuation of Figure 2

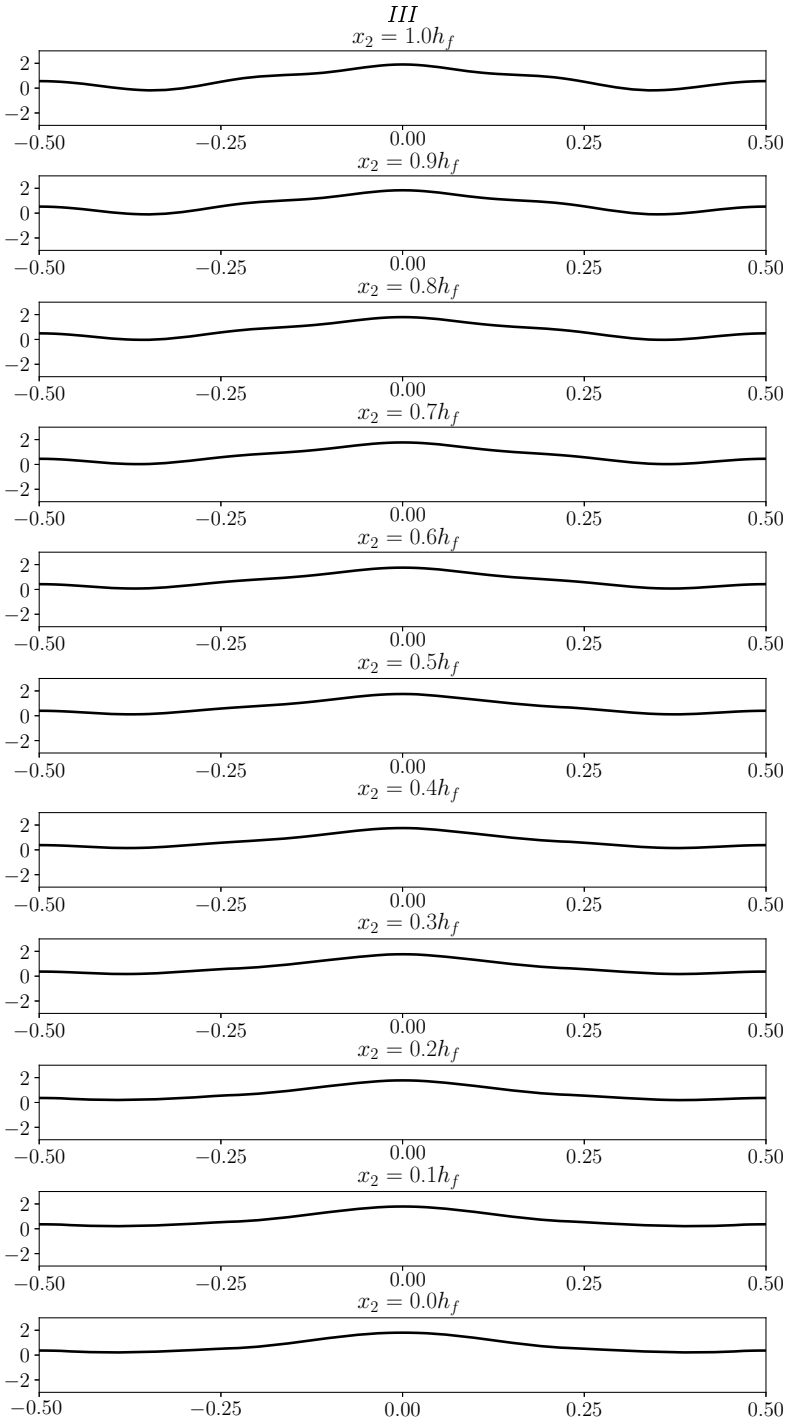


Continuation

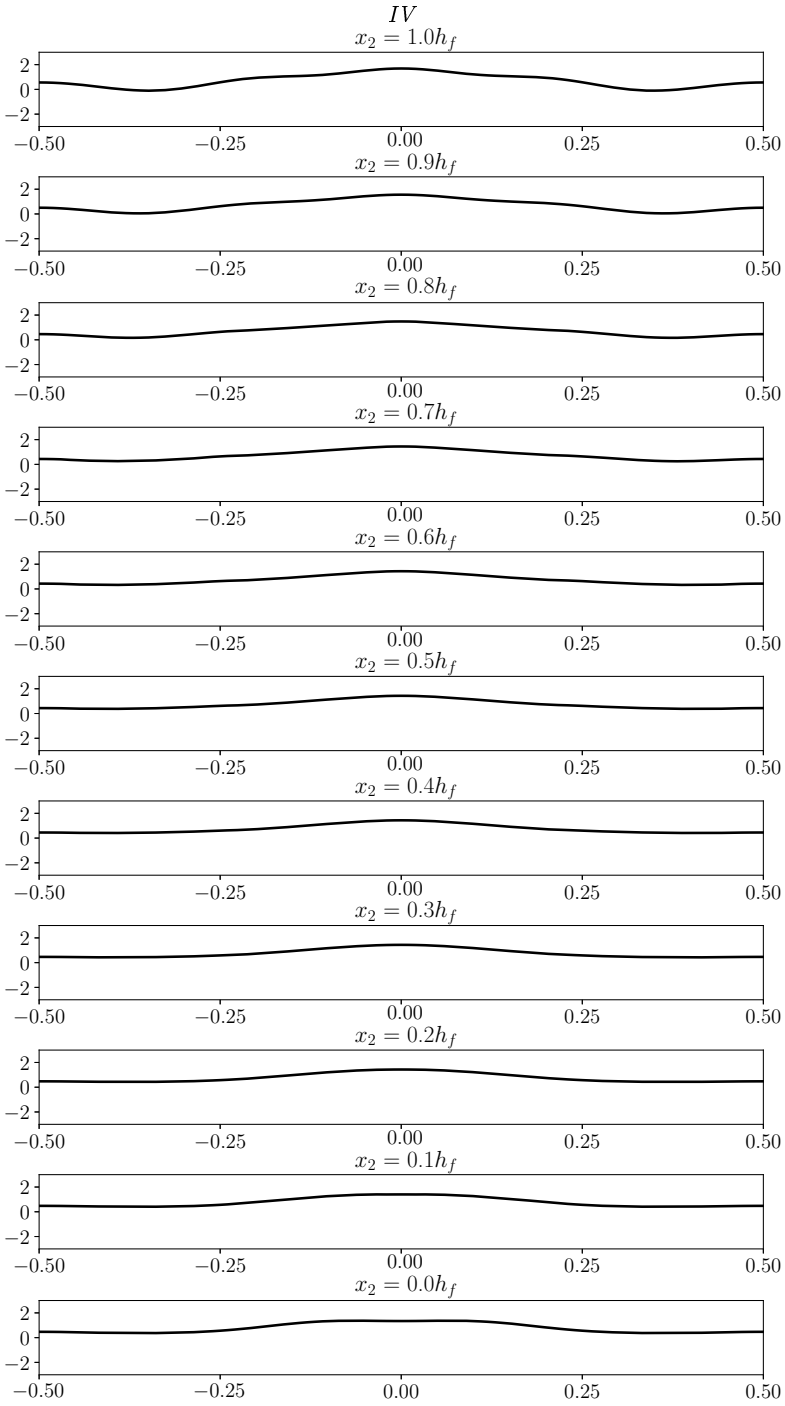
IV
$x_2 = 1.0h_f$
$x_2 = 0.9h_f$
$x_2 = 0.8h_f$
$x_2 = 0.7h_f$
$x_2 = 0.6h_f$
$x_2 = 0.5h_f$
$x_2 = 0.4h_f$
$x_2 = 0.3h_f$
$x_2 = 0.2h_f$
$x_2 = 0.1h_f$
$x_2 = 0.0h_f$
2
0
−2
−0.50
−0.25
0.00
0.25
0.50

of Figure 2

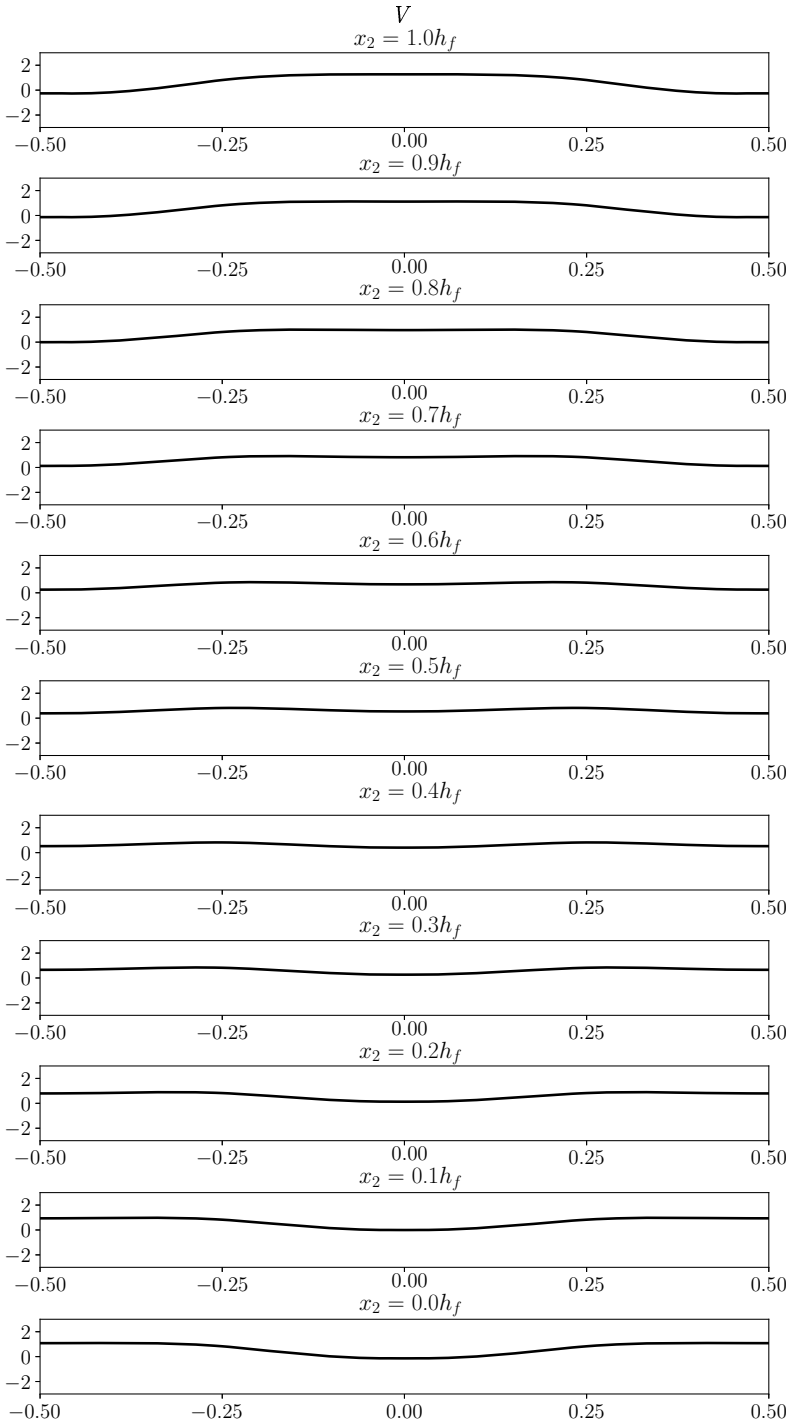


Continuation

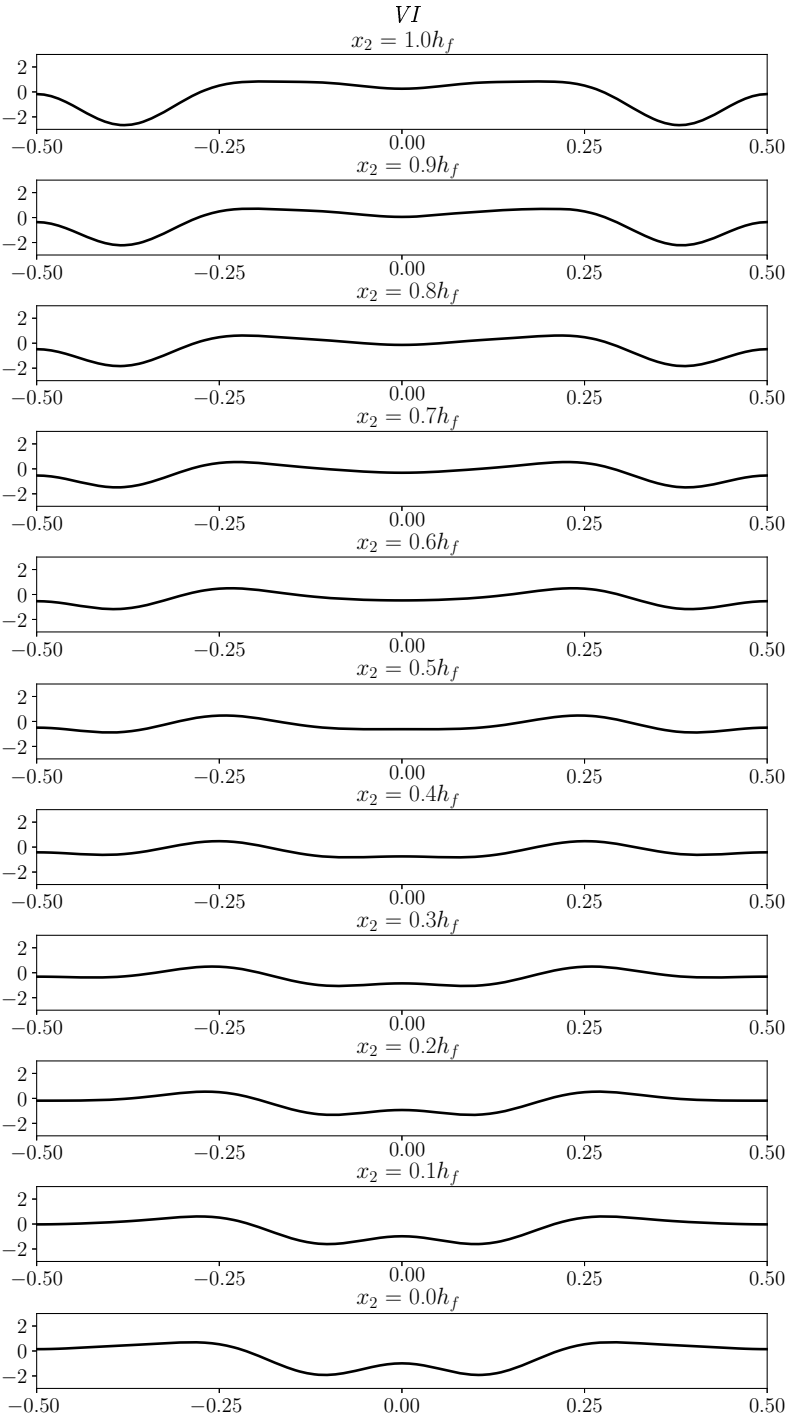
VI
$x_2 = 1.0h_f$
$x_2 = 0.9h_f$
$x_2 = 0.8h_f$
$x_2 = 0.7h_f$
$x_2 = 0.6h_f$
$x_2 = 0.5h_f$
$x_2 = 0.4h_f$
$x_2 = 0.3h_f$
$x_2 = 0.2h_f$
$x_2 = 0.1h_f$
$x_2 = 0.0h_f$
2
0
−2
−0.50
−0.25
0.00
0.25
0.50

of Figure 2

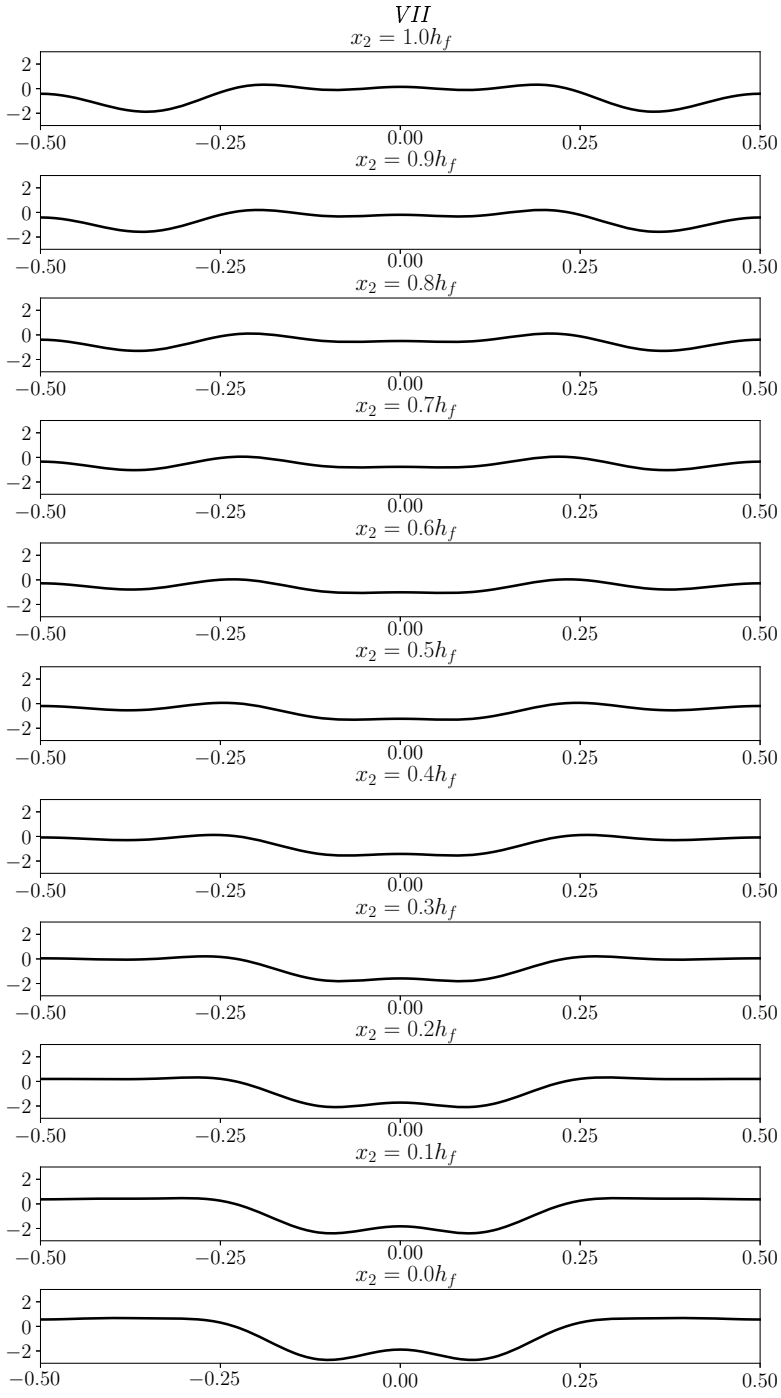
VII
$x_2 = 1.0h_f$
$x_2 = 0.9h_f$
$x_2 = 0.8h_f$
$x_2 = 0.7h_f$
$x_2 = 0.6h_f$
$x_2 = 0.5h_f$
$x_2 = 0.4h_f$
$x_2 = 0.3h_f$
$x_2 = 0.2h_f$
$x_2 = 0.1h_f$
$x_2 = 0.0h_f$
2
0
−2
−0.50
−0.25
0.00
0.25
0.50

End

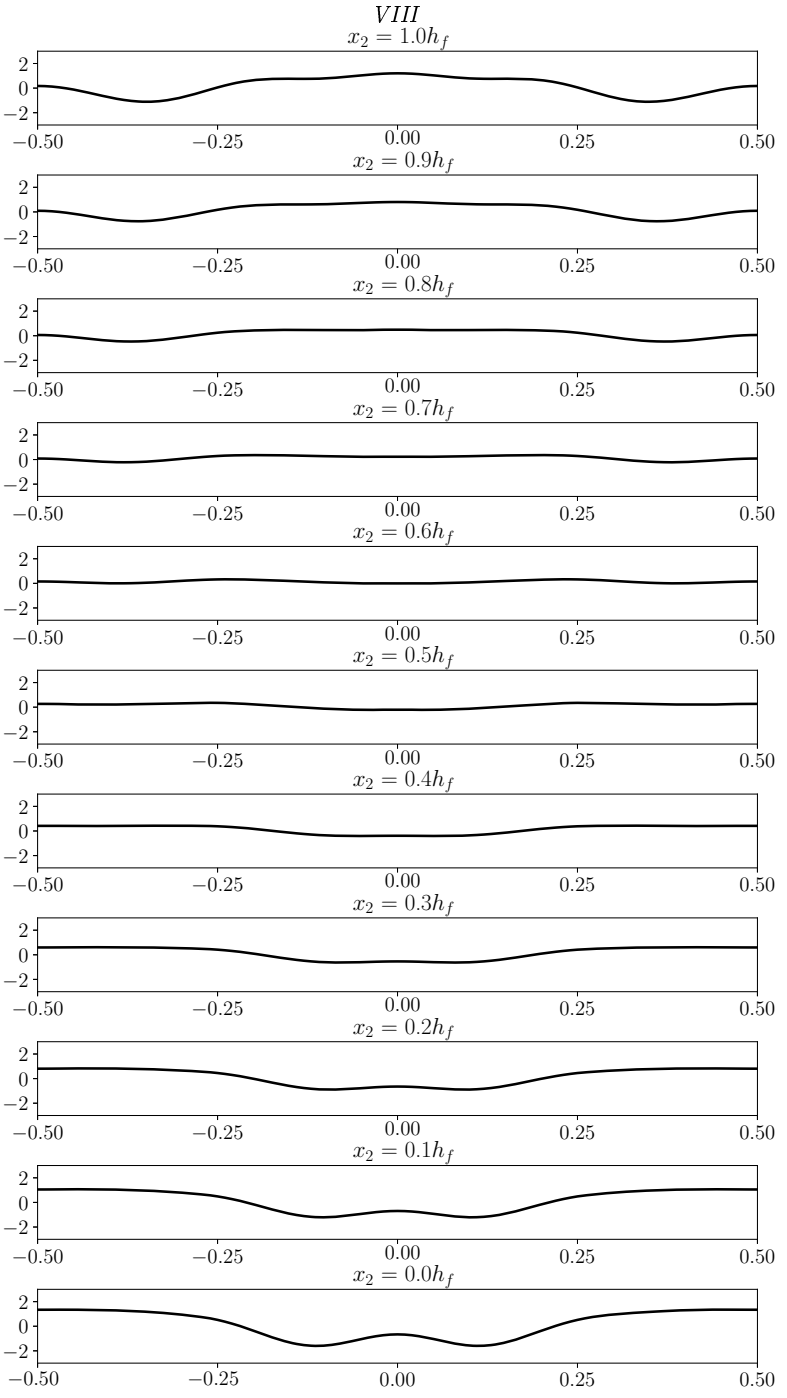
VIII
$x_2 = 1.0h_f$
$x_2 = 0.9h_f$
$x_2 = 0.8h_f$
$x_2 = 0.7h_f$
$x_2 = 0.6h_f$
$x_2 = 0.5h_f$
$x_2 = 0.4h_f$
$x_2 = 0.3h_f$
$x_2 = 0.2h_f$
$x_2 = 0.1h_f$
$x_2 = 0.0h_f$
2
0
−2
−0.50
−0.25
0.00
0.25
0.50

of Figure 2

To map the presented stress distribution on sound, we scale the stress level to $[-1, 1]$ range and directly translate it to the audible domain. Thus, the sound signal $s$ can be presented as

$$s(t) = \sum_{k=1}^{5} \widetilde{A_k}(x_2, h_f, A, f_0, r, M_1^s, M_2^s) \cos(2\pi k f_0 t), \tag{9}$$

where the fundamental frequency of the generated sound $f_0$ is obtained by mapping the film undulation wavelength defined in the range $a \in [1, 1000]$ nm to sound wavelength defined in the range $\lambda \in [0.017, 17.15]$ m under consideration the speed of sound equal to $v = 343$ m/s which corresponds to the range of human hearing frequency perception $f_0 \in [20, 20\,000]$ Hz. It is worth noting that the harmonic amplitudes are varying with the fundamental frequency variation due to the size effect observed in nanoscale systems. For the wrinkled ultra-thin films with sinusoidal geometry, it was analysed in [30]. Modulating the parameter $x_2$, we get the sound morphing effect graphically presented in Figures 2, *I–VIII*. The modulation rate can be linked with the film thickness $h_f$ in such a way that the increasing of the parameter $h_f$ leads to decreasing the modulation rate.

As an example, one can see a diagram of a sound waveform presented in Figure 3 within one period which is corresponded to the scaled distribution of the normalized longitudinal stress $\sigma_{tt}/T_1$ in the film along the lines $x_2 = h_f$ (Figure 3, *a*) and $x_2 = 0$ (Figure 3, *b*) within one period $x_1/a = [-0.5, 0.5]$ in the case of the film-substrate system described by the following parameters: $a = 10$ nm, $A = 0.1a$, $h_f = 0.2a$, $r = 10$, $M_1^s = 10$ N/m, $M_2^s = 10$ N/m.

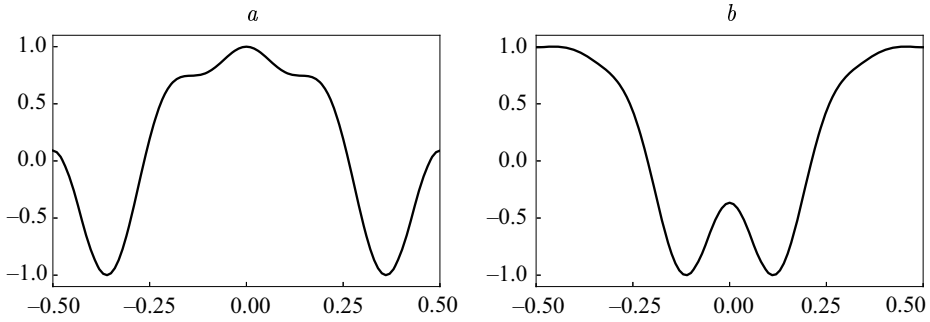


*Figure 3.* Diagram of a sound waveform within one period which is corresponded to the scaled distribution of the normalized longitudinal stress $\sigma_{tt}/T_1$ in the film along the lines $x_2 = h_f$ (*a*) and $x_2 = 0$ (*b*) within one period $x_1/a = [-0.5, 0.5]$ in the case of the film-substrate system described by the parameters $a = 10$ nm, $A = 0.1a$, $h_f = 0.2a$, $r = 10$, $M_1^s = 10$ N/m, $M_2^s = 10$ N/m

**4. Conclusion**. In this paper, the model of a wrinkled thin film coating describing the undulation of the elastic stress field caused by the perturbed film geometry was employed for the development of a sound synthesis algorithm. The film-on-substrate structure was considered as a multilevel system where the elastic properties of the surface and interphase layers differ from the similar properties of the bulk phases. The superposition of two perturbed stress fields raised as a result of surface and interface geometric imperfections leads to interference patterns in the stress field within the bulk phase of the film coating. The analysis of the periodic stress distribution in the thin film along the lines parallel to the unperturbed surface/interface boundaries allowed us to map the stress oscillations smoothly changing from surface to interface to the sound waveforms with rich

morphologies. Modulation through the thickness of the film results in the sound morphing effect.

The presented model is based on the semi-analytical solution obtained using symbolic computations, and it is not suitable for real-time interactive simulation. In order to overcome this issue, we are going to employ the neural network with feedforward architecture trained on data generated on the basis of the derived solution. The design of the neural network capable of reconstructing the Fourier series coefficients using the geometrical and physical parameters of the discussed problem is the objective of future research.

**References**


1. Bilbao S. *Numerical sound synthesis: finite difference schemes and simulation in musical acoustics*. Chichester, John Wiley & Sons Publ., 2009, 456 p.

2. Borin G., Poli G. D., Sarti A. Algorithms and structures for synthesis using physical models. *Computer Music Journal*, 1992, vol. 16, pp. 30–42.

3. Castagné N., Cadoz C. A goals-based review of physical modelling. *International Computer Music Conference*, 2005, pp. 343–346.

4. Smith J. O. Physical modeling using digital waveguides. *Computer Music Journal*, 1992, vol. 16, pp. 74–91.

5. Najnudel J., Hélie T., Roze D. Simulation of the Ondes Martenot ribbon-controlled oscillator using energy-balanced modeling of nonlinear time-varying electronic components. *Journal of the Audio Engineering Society*, 2019, vol. 67, pp. 961–971.

6. Najnudel J., Hélie T., Roze D., Müller R. Power-balanced modeling of nonlinear coils and transformers for audio circuits. *Journal of the Audio Engineering Society*, 2021, vol. 69, pp. 506–516.

7. Chabassier J., Chaigne A., Joly P. Modeling and simulation of a grand piano. *The Journal of the Acoustical Society of America*, 2013, vol. 134, pp. 648–665.

8. Ducceschi M., Bilbao S. Simulation of the geometrically exact nonlinear string via energy quadratisation. *Journal of Sound and Vibration*, 2022, vol. 534, p. 117021.

9. Hamilton B., Bilbao S. Time-domain modeling of wave-based room acoustics including viscothermal and relaxation effects in air. *JASA Express Letters*, 2021, vol. 1, p. 092401.

10. Bilbao S., Hamilton B. Wave-based room acoustics simulation: explicit/implicit finite volume modeling of viscothermal losses and frequency-dependent boundaries. *Journal of the Audio Engineering Society*, 2017, vol. 65, pp. 78–89.

11. Cadoz C. The physical model as metaphor for musical creation: pico.. TERA, a piece entirely generated by physical model. *International Computer Music Conference*, 2002, pp. 305–312.

12. Chafe C. Case studies of physical models in music composition. *Proceedings of the $18^{th}$ International Congress on Acoustics*, 2004, pp. 2505–2508.

13. Sturm B. L. Composing for an ensemble of atoms: the metamorphosis of scientific experiment into music. *Organised Sound*, 2001, vol. 6, pp. 131–145.

14. Vinjar A. Bending common music with physical models. *International Conference on New Interfaces for Musical Expression*, 2008, pp. 335–338.

15. Nierhaus G. *Algorithmic composition: paradigms of automated music generation*. Wien, Springer Publ., 2009, 287 p.

16. Roads C. *Composing electronic music: a new aesthetic*. New York, Oxford University Press, 2015, 512 p.

17. Freund L. B., Suresh S. *Thin film materials: stress, defect formation and surface evolution*. Cambridge, Cambridge University Press, 2004, 770 p.

18. Lüth H. *Solid surfaces, interfaces and thin films*. Berlin, Springer Publ., 2001, 589 p.

19. Eremeyev V. A. On effective properties of materials at the nano- and microscales considering surface effects. *Acta Mechanica*, 2016, vol. 227, pp. 29–42.

20. Javili A., McBride A., Steinmann P. Thermomechanics of solids with lower-dimensional energetics: on the importance of surface, interface, and curve structures at the nanoscale. A unifying review. *Applied Mechanics Reviews*, 2013, vol. 65, p. 010802.

21. Mogilevskaya S. G., Crouch S. L., La Grotta A., Stolarski H. K. The effects of surface elasticity and surface tension on the transverse overall elastic behavior of unidirectional nanocomposites. *Composites Science and Technology*, 2010, vol. 70 pp. 427–434.

22. Sharma P., Ganti S., Bhate N. Effect of surfaces on the size-dependent elastic state of nanoinhomogeneities. *Applied Physics Letters*, 2003, vol. 82, pp. 535–537.

23. Wang J., Huang Z., Duan H., Yu S., Feng X., Wang G., Zhang W., Wang T. Surface stress effect in mechanics of nanostructured materials. *Acta Mechanica Solida Sinica*, 2011, vol. 24, pp. 52–82.

24. Povstenko Y. Z. Theoretical investigation of phenomena caused by heterogeneous surface tension in solids. *Journal of the Mechanics and Physics of Solids*, 1993, vol. 41, pp. 1499–1514.

25. Duan H. L., Wang J., Karihaloo B. L. Theory of elasticity at the nanoscale. *Advances in Applied Mechanics*, 2001, vol. 42, pp. 1–68.

26. Miller R. E., Shenoy V. B. Size-dependent elastic properties of nanosized structural elements. *Nanotechnology*, 2000, vol. 11, pp. 139–147.

27. Kostyrko S. A., Altenbach H., Grekov M. A. Stress concentration in ultra-thin coating with undulated surface profile. *VII International Conference on Computational Methods for Coupled Problems in Science and Engineering*, 2017, pp. 1183–1192.

28. Kostyrko S. A., Grekov M. A., Altenbach H. A model of nanosized thin film coating with sinusoidal interface. *AIP Conference Proceedings*, 2018, vol. 1959, p. 070017.

29. Kostyrko S. A., Grekov M. A., Altenbach H. Stress concentration analysis of nanosized thin-film coating with rough interface. *Continuum Mechanics and Thermodynamics*, 2019, vol. 31, pp. 1863–1871.

30. Kostyrko S. A., Grekov M. A., Altenbach H. Coupled effect of curved surface and interface on stress state of wrinkled thin film coating at the nanoscale. *ZAMM — Journal of Applied Mathematics and Mechanics*, 2021, vol. 101, p. e202000202.

31. Shuvalov G. M., Vakaeva A. B., Shamsutdinov D. A., Kostyrko S. A. The effect of nonlinear terms in boundary perturbation method on stress concentration near the nanopatterned bimaterial interface. *Vestnik of Saint Petersburg University. Applied Mathematics. Computer Sciences. Control Processes*, 2020, vol. 16, iss. 2, pp. 165–176. https://doi.org/10.21638/11701/spbu10.2020.208

32. Kim H.-K., Lee S.-H., Yao Z., Wang C., Kim N.-Y., Kim S. I., Lee C. W., Lee Y.-H. Suppression of interface roughness between $BaTiO_3$ film and substrate by $Si_3N_4$ buffer layer regarding aerosol deposition process. *Journal of Alloys and Compounds*, 2015, vol. 653, pp. 69–76.

33. Romanova V. A., Balokhonov R. R. Numerical analysis of mesoscale surface roughening in a coated plate. *Computational Materials Science*, 2012, vol. 61, pp. 71–75.

34. Javili A., Bakiler A. D. A displacement-based approach to geometric instabilities of a film on a substrate. *Mathematics and Mechanics of Solids*, 2019, vol. 24, pp. 2999–3023.

35. Nikravesh S., Ryu D., Shen Y.-L. Direct numerical simulation of buckling instability of thin films on a compliant substrate. *Advances in Mechanical Engineering*, 2019, vol. 11, pp. 1–15.

36. Kostyrko S., Shuvalov G. Surface elasticity effect on diffusional growth of surface defects in strained solids. *Continuum Mechanics and Thermodynamics*, 2019, vol. 31, p. 1795001803.

37. Shuvalov G., Kostyrko S. On the role of interfacial elasticity in morphological instability of a heteroepitaxial interface. *Continuum Mechanics and Thermodynamics*, 2021, vol. 33, pp. 2095–2107.

38. Shuvalov G. M., Kostyrko S. A. Stability analysis of a nanopatterned bimaterial interface. *Vestnik of Saint Petersburg University. Applied Mathematics. Computer Sciences. Control Processes*, 2021, vol. 17, iss. 1, pp. 97–104. https://doi.org/10.21638/11701/spbu10.2021.109

39. Wu C. H. The chemical potential for stress-driven surface diffusion. *Journal of the Mechanics and Physics of Solids*, 1996, vol. 44, pp. 2059–2077.

40. Gurtin M. E., Murdoch I. A. A continuum theory of elastic material surfaces. *Archive for rational mechanics and analysis*, 1975, vol. 57, pp. 291–323.

41. Gurtin M. E., Murdoch I. A. Surface stress in solids. *International Journal of Solids and Structures*, 1978, vol. 14, pp. 431–440.

42. Chen T. , Chiu M.-S., Weng C.-N. Derivation of the generalized Young — Laplace equation of curved interfaces in nanoscaled solids. *Journal of Applied Physics*, 2006, vol. 100, p. 074308.

43. Grekov M. A. *Singuliarnaia ploskaia zadacha teorii uprugosti* [*Singular plane problems in elasticity*]. St. Petersburg, St. Petersburg University Press, 2001, 192 p. (In Russian)

44. Kolosov G. V. *Primenenie kompleksnykh diagramm i teorii funktsii kompleksnoi peremennoi k teorii uprugosti* [*Application of complex diagrams and the theory of functions of a complex variable to the theory of elasticity*]. Moscow, Gostekhizdat Publ., 1935, 224 p. (In Russian)

45. Muskhelishvili N. I. *Some basic problems of the mathematical theory of elasticity*. Groningen, P. Noordhoff Ltd. Publ., 1963, 732 p.

46. Nayfeh A. H. *Perturbation methods*. Wienheim, John Wiley & Sons Publ., 2008, 440 p.

47. Osaka N. Timbre morphing and interpolation based on a sinusoidal model. *The Journal of the Acoustical Society of America*, 1998, vol. 103, p. 2757.

48. Tellman E., Haken L., Holloway B. Timbre morphing of sounds with unequal numbers of features. *Journal of the Audio Engineering Society*, 1995, vol. 43, pp. 678–689.

49. Grekov M. A., Kostyrko S. A. Surface effects in an elastic solid with nanosized surface asperities. *International Journal of Solids and Structures*, 2016, vol. 96, pp. 153–161.

50. Kostyrko S. A., Grekov M. A. Elastic field at a rugous interface of a bimaterial with surface effects. *Engineering Fracture Mechanics*, 2019, vol. 216, p. 106507.

51. Mikhlin S. G. *Integral equations: and their applications to certain problems in mechanics, mathematical physics and technology.* New York, Pergamon Press, 1964, 338 p.

52. Shenoy V. B. Atomistic calculations of elastic properties of metallic fcc crystal surfaces. *Physical Review B*, 2005, vol. 71, p. 094104.

Received: December 14, 2022.
Accepted: January 19, 2023.

Authors' information:

*Sergey A. Kostyrko* — PhD in Physics and Mathematics, Associate Professor; sergey.kostyrko@gmail.com

*Boris S. Shershenkov* — PhD in Technical Sciences; boris.shershenkov@list.ru

## Метод синтеза звука, основанный на анализе упругих напряжений в гофрированном тонкопленочном покрытии*

*С. А. Костырко, Б. С. Шершенков*

Университет ИТМО, Российская Федерация,
197101, Санкт-Петербург, Кронверский пр., 49

**Для цитирования:** *Kostyrko S. A., Shershenkov B. S.* Sound synthesis approach based on the elastic stress analysis of a wrinkled thin film coating // Вестник Санкт-Петербургского университета. Прикладная математика. Информатика. Процессы управления. 2023. Т. 19. Вып. 1. С. 72–89. https://doi.org/10.21638/11701/spbu10.2023.107

Изучается возможность использования модели гофрированного тонкопленочного покрытия в условиях плоской деформации для генерации и манипулирования звуком. Структура «пленка — подложка» рассматривается как многоуровневая система, в которой упругие свойства поверхностных и межфазных слоев отличаются от аналогичных свойств объемных фаз. Суперпозиция двух возмущенных полей напряжений, возникших в результате геометрических несовершенств поверхности и межфазного слоя, демонстрирует интерференционные картины поля напряжений в объемной фазе пленочного покрытия. Анализ периодического распределения напряжений в тонкой пленке вдоль линий, параллельных невозмущенным границам поверхности/интерфейса, приводит к развитию различных форм волн, плавно переходящих от поверхности к интерфейсу. Такое наблюдение позволяет сформулировать метод синтеза звука, аналогичный методу тембрального морфинга, который обеспечивает переход между двумя звуками, создавая в ходе этого процесса новые промежуточные звуки. Перспективность использования модели гофрированной тонкой пленки для генерации звука обусловлена ее сложным поведением, когда в ходе анализа напряженного состояния влияние одного параметра отражается на влияние других, что, в свою очередь, приводит к различным звуковым морфологиям.

*Ключевые слова*: синтез звука, физическое моделирование, гофрированное тонкопленочное покрытие, возмущение поля напряжений.

Контактная информация:

*Костырко Сергей Алексеевич* — канд. физ.-мат. наук, доц.; sergey.kostyrko@gmail.com

*Шершенков Борис Сергеевич* — канд. техн. наук; boris.shershenkov@list.ru

* Работа выполнена в рамках стипендиальной программы Университета ИТМО.